PCCP

Accepted Manuscript

ROYAL SOCIETY OF CHEMISTRY

www.rsc.org/pccp

WAVELENGTH DISPERSION OF THE LOCAL FIELD INTENSITY IN SILVER-GOLD NANOCAGES

R. Pilot,*[a] A. Zoppi,[b‡] S. Trigari,[b] F. L. Deepak,[c] E. Giorgetti[b] and R. Bozio[a]

[a] Consorzio INSTM and Department of Chemical Sciences, via Marzolo 1, 35131 Padova, Italy

[b] ISC CNR Via Madonna del Piano 10, Sesto Fiorentino (Firenze), Italy

[c] International Iberian Nanotechnology Laboratory, Avenida Mestre Jose Veiga, Braga 4715-330, Portugal

‡ present address: Physics Department, University of Pisa, Largo B. Pontecorvo 3, 56127 Pisa, Italy

***corresponding author**

ABSTRACT

This study provides a combined theoretical and experimental analysis of the far-field (extinction) and of the near-field (SERS enhancement) spectral distribution in hollow nanoparticles, that is silver-gold nanocages (NCs). Chitosan protected NCs have been synthesized by a galvanic replacement-based procedure: their morphological properties and chemical composition have been characterized by TEM, STEM and ICP. NCs were then functionalized with a thiolated organic dye prior to carrying out SERS measurements.

Finite Element Method simulations of a single NC have shown that the field enhancement at the excitation wavelength follows the same spectral dependence as the extinction spectrum and, consequently, the SERS enhancement profile, as a function of the excitation wavelength, peaks at higher energy with respect to extinction. The simulated extinction is remarkably narrower than the experimental spectrum of NCs in solution, indicating that the colloidal sample is substantially polydispersed. However, a simple qualitative model we developed would suggest that the SERS enhancement profile is blue-shifted with respect to the extinction in the presence of polydispersivity as well.

Also NC dimers have been simulated: both their extinction and near field-spectra shift to the red when the size of the gap is reduced, in analogy to what happens with dimers of filled spherical nanoparticles (NPs). In addition, simulations also revealed that a NC dimer is only slightly more efficient in amplifying the field with respect to the isolated NC: this behavior is peculiar to NCs, in fact filled spherical NP dimers exhibit a remarkably stronger field enhancement with respect to the isolated NP.

By means of Wavelength Scanned SERS, we measured the spectral distribution of the local field in a dispersion of NCs: we observed experimentally that the local field is distributed in the same spectral region as the extinction and that the absolute value of the SERS enhancement factor maintains a low value throughout the range explored (568-800 nm).

We propose that the observed correlation between the SERS profile and the extinction is accidental and originates from the limited increase in amplification provided by NC aggregates with respect to isolated NCs.

1. Introduction

Noble metals nanostructures have gained widespread attention from the scientific community, due to their unique physical and optical properties that have been exploited in a lot of fields, including medical diagnostics, drug delivery and smart materials.[1,2,3,4] The wealth of their possible applications has driven an intense research effort aimed at tailoring the nanostructure properties to the specific fields of employment.

In this regard, an important class of nanoparticles (NPs) is represented by hollow NPs and, among them, by nanocages (NCs), whose characteristic signatures are the empty interior and the porous walls, that make them attractive for drug delivery applications.[5,6] In addition, their extinction spectrum is tunable, as a function of their structural details, from the visible to the near-infrared, where the absorption of hemoglobin and biological tissues is negligible: this feature has opened the way to their use in the biomedical field,[7,8] specifically in diagnostics and photothermal tumor therapy.[9,10,11] Moreover, in analogy to their filled counterparts, hollow NPs exhibit a plasmonic behavior, that is their free electrons can oscillate coherently in response to a resonant external electromagnetic field. This phenomenon brings along a strong intensification of the electromagnetic field at the surface of the NPs, making them exploitable in surface enhanced spectroscopy, in particular Surface Enhanced Raman Scattering (SERS).[6,12,13,14] For instance, SERS has been used to simultaneously control and monitor the polymerization process of diacetylene layers adsorbed on Au-Ag NCs.[15,16] The fact that hollow NPs combine in a single object different functionalities has also stimulated their study in simultaneous therapeutic and diagnostic applications (i.e. theranostic).[6,9,17]

Focusing on the optical properties, and in particular on surface enhanced spectroscopy, a lot of effort has been spent in recent years to figure out the interplay between the optical far-field (extinction) and the near-field (local field) response of metal nanostructures. The basic problem to address is whether or not the excitation wavelength dependence of the Raman enhancement is predictable on the basis of the extinction/absorption features of the sample, and therefore if a guideline exists indicating the spectral region with the maximum SERS activity. This issue has been tackled by electromagnetic modeling[18,19] and Wavelength Scanned SERS (WS-SERS) experiments, namely the measurement of the local field enhancement at several wavelengths in order to build its spectral profile.[19,20,21] It is worth mentioning that WS-SERS studies are not so

common in the literature, due to the fact that they require a very specialized setup, equipped with tunable laser sources and a tunable detection system in order to collect a sufficient number of points to build the SERS Enhancement Factor (EF) profile. Currently, it is commonly accepted that, at least in metal NPs of conveniently small size, the near-field intensity should track the extinction/absorption spectrum. For instance, the simulations carried out by Messinger[22] show that the extinction, scattering, absorption and near-field cross section of gold and silver nanoparticles, with diameters around 40 nm, follow the same spectral dependence and that they peak at approximately the same wavelength. Some experimental studies have investigated, instead of single nanoparticles, more complex systems composed by an ordered ensemble of ideally identical objects. Demonstration of correlation between extinction/absorbance and SERS enhancement was provided by McFarland[20] on an ordered array of nanotriangles (fabricated by nanosphere lithography) and by Felidj[23] on a regular array of elongated gold nanoparticles (fabricated by electron-beam lithography). Mc Farland also demonstrated in his system that the SERS EF profile, plotted versus the excitation wavelength, peaked at higher energy with respect to the extinction.

However, things become more complicated when strongly coupled systems (e.g. dimers with a small gap) are involved. As pointed out by Le Ru[18] *bulk-like* resonances, proportional to volume, can bring along a strong contribution to the absorption/scattering but are not necessarily related to strong localization of light on the surface at a specific point; on the other hand, *surface-like* resonances may not produce remarkable far-field effects but they are possibly related to a strong intensification at some points of the surface. A very clear experimental and theoretical demonstration of the fact that in single isolated gold dimers the local field profile shows very little dependence on the far-field is provided in the paper by Kleinman.[19]

In addition, a complete lack of correlation is typically experienced in colloidal solutions of gold or silver NPs functionalized with Raman active species. In these cases, the SERS enhancement appears at longer wavelengths with respect to extinction.[24,25,26,27,28] These data can be interpreted in the light of the presence of a small amount of aggregates in solution that do not significantly influence the extinction spectra, but are very efficient in amplifying the Raman scattering. Moskovits[29] commented that dimers and larger aggregates produce enhancements which are five-to-six orders of magnitude larger than single isolated

nanoparticles and, therefore, even a tiny amount of them overwhelms the SERS from isolated nanoparticles.

Within this framework, the purpose of this paper was to investigate the spectral distribution of the local field enhancement in a particular type of hollow and porous NPs (namely silver/gold nanocages, NCs).

To the best of our knowledge, the spectral distribution of the near-field intensity has never been investigated in NCs, nor compared to the far-field spectra. Therefore, in this work, we present a WS-SERS study of NCs functionalized with a SERS active thiolated molecule. We compare the results of SERS experiments, on one side, with the measured extinction spectrum of the nanostructures and, on the other side, with the theoretical results obtained with a model that we developed, which is based on a Finite Element Method-(FEM) computer code and permits the simulation of the electromagnetic properties of the NCs.[30] This would also represent a guideline for testing the ability of theoretical/computational models to treat relatively complex nanostructures. In addition to giving a contribution to the understanding of a basic issue, which has been debated in the literature but, up to now, tackled only by a limited number of papers, we think that our study can also have practical implications in fields where NCs, or hollow NPs in general, are exploited as carriers, e.g., in drug delivery applications, while monitoring the transport process by surface enhanced spectroscopies.

2. Experimental and theoretical methods

Chemicals and materials

$AgNO_3$ was purchased from Merck and $NaBH_4$, $HAuCl_4$, acetone were purchased from Sigma Aldrich. High molecular weight chitosan (~10^6 Da) was obtained from Heppe Medical. Ultrapure water (resistivity 18 MΩ·cm) was used as solvent in all experiments. All the glassware was cleaned with *piranha* solution.

The test molecule used for NCs functionalization is the N-substituted fluorescent derivative of 4-methoxy-1,8-naphtalimide (NAFTA6) whose structure is reported in Figure 1. NAFTA6 was provided by the Institute of Organic Chemistry with Centre of Phytochemistry (BAS) in Sofia, Bulgaria.[31]

A regenerated cellulose tubing (Visking) with a cut-off of 12-14 kDa was used for dialysis purification of the functionalized NCs, with a buffer to sample volume ratio 10:1.

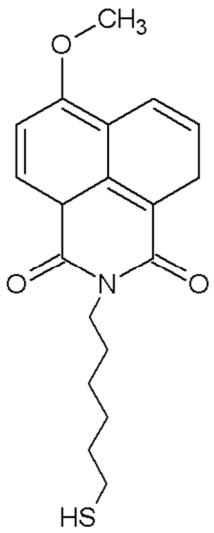

Figure 1: Molecular structure of the reporter molecule NAFTA6.

Synthesis of NCs

The synthesis of the NCs was performed according to a galvanic replacement-based procedure, as described in Refs. 7, 10, 15. We used chitosan as the stabilizing and protecting agent. First, chitosan-capped Ag nanoparticles (AgNPs) were synthesized by adding to 4.3 ml of a 9.5 mM chitosan 1%-acetic acid solution 4.2 ml of H_2O and 0.8 ml of 45 mM $AgNO_3$. The mixture was vigorously stirred before adding 0.63 ml of 57 mM $NaBH_4$. The reaction occurred

at ambient temperature in an amber-glass vial under moderate stirring. Subsequently, 1.5 ml of the AgNPs seeds were diluted in a volumetric flask with 12.5 ml of water and heated up till 70°C. Then, $HAuCl_4$ was added under vigorous stirring according to a n_{Ag}/n_{Au} = 5.3 molar rate. After few minutes, the hot plate was removed, the flask was left to cool down and the final NCs colloidal solution was kept on shelf at room temperature.

Surface modification of NCs

For surface modification of the NCs, NAFTA6 was dissolved in pure acetone and added to the colloidal suspension of NCs in order to achieve a final molar NAFTA6/Au rate equal to 0.7 and a H_2O:acetone rate equal to 5:1. The reaction was let to undergo overnight undisturbed. The modified NAFTA6-NC suspension was then purified by dialysis in order to remove the reporter molecule not bound to the metallic structures. To this aim, the solution was inserted in a dialysis membrane and immersed in a 10-fold larger volume of a 5:1 H_2O:acetone solution. The external solution was changed three times during the next 23 hours. The overall amount of NAFTA6 washed out by dialysis was quantitatively estimated by fluorescence spectroscopy using a calibration curve (not reported here) obtained by dissolving known quantities of NAFTA6 in a 5:1 H_2O:acetone mixture. The amount of NAFTA6 in the dialyzed sample was thus evaluated by difference between the initial amount of the reporter molecule and the extracted one.

Optical and morphological characterization

Extinction and fluorescence spectra were acquired using 1 cm path length quartz cuvettes with a Cary 5 spectrometer and a Perkin-Elmer LS55 spectro-photo-fluorimeter equipped with a high-energy Pulsed Xenon source, respectively.

The composition of Au/Ag NCs was studied using a Varian 720-ES inductively coupled plasma atomic emission spectrometer (ICP-AES). To this purpose, a small aliquot (0.1 ml) of the dialyzed colloid solution was digested with 2 ml of *aqua regia* and kept at 75°C for 24 h before analysis.

TEM images were obtained with a Philips CM12 cryo-gatan UHRST 3500 operating at 100 kV. The samples were prepared by wetting carbon-coated Cu grids with a drop of colloid and letting the solvent to evaporate at room temperature. Morphologic parameters (diameter

and shell thickness) were evaluated by fitting with Log-Normal functions the histograms obtained over about one-hundred particles.

The same grids were used for high resolution (HR) TEM and scanning TEM (STEM) analysis, which were carried out with a Titan ChemiSTEM 80-200 kV probe Cs corrected microscope and equipped with a Super-X EDS System. Low-magnification TEM and high-resolution TEM (HRTEM) images were acquired with a GATAN ULTRASCAN 1000 P camera controlled with a Digital Micrograph software integrated in the microscope user interface. STEM images were acquired with a high angle annular dark field (HAADF) detector. The alignment of the microscope was carried out through the Cs DCOR probe corrector software. EDS spectra and elemental maps were acquired with the Super-X EDS system.

Theoretical modelling

Theoretical 3D simulations were carried out by a commercially available FEM package (COMSOL Multiphysics), which allows to solve numerically the near and far fields of the tested nanostructures and, eventually, their extinction efficiencies and electromagnetic field distributions close to the surface.[30]

Raman and SERS measurements

A home-made Macro-Raman setup was used to carry out Wavelength Scanned SERS measurements. This system is equipped with a CW Ti:Sapphire Laser tunable in the 675nm - 1000nm range (Spectra Physics, 3900S) and pumped by a CW Optically Pumped Semiconductor Laser (Coherent, Verdi G7) and an Ar^+/Kr^+ gas laser (Coherent, Innova 70) providing as principal lines 488 nm, 514.5 nm and 647.1 nm. Laser beams are filtered through a tunable laser plasma line filter monochromator (Laserspec III, Spectrolab) and focused on the sample through a cylindrical lens. The Raman scattering diffused by the sample is collected by a camera objective (CANON 50 mm, f/1.2) and imaged through the slit of a three stage subtractive spectrograph (Jobin Yvon S3000), made up by a double monochromator (Jobin Yvon, DHR 320) working as a tunable filter and a spectrograph (Jobin Yvon HR 640). The Raman signal is detected by a liquid nitrogen cooled CCD detector (Jobin Yvon, Symphony). A polarization scrambler is mounted in between the collection objective and the spectrograph slit. The system is configured in backscattering configuration by placing a tiny mirror right in front of the collection objective to steer the beam from the cylindrical lens to the

sample. The sample is mounted on a translation stage that allows one to move it parallel and perpendicular with respect to the laser propagation direction. The size of the laser at the sample is about 3 mm by 80 μm and the axial collection efficiency was measured to be around 3 mm. The power at the sample was about 200 mW for the NIR wavelengths and about 12 mW for the visible wavelengths, corresponding to intensities of 80 W/cm^2 and 8 W/cm^2, respectively. All measurements were accomplished in solution in 1cm-thick cuvettes.

3. Results

Optical and morphological characterization

Suspensions of chitosan-protected NCs were prepared and subsequently functionalized with NAFTA6. The concentration of NAFTA6 conjugated to the NCs was estimated to be 4×10^{-5} M, according to the procedure illustrated in section 2.

Figure 2 reports the experimental extinction spectra of the NCs before (solid black line) and after (solid red line) functionalization. The initial extinction band of the NCs is peaked at 748 nm and red-shifts to 754 nm after conjugation with the NAFTA6 reporter molecule. The typical absorption of NAFTA6, centered at 374 nm, is also visible. The dashed lines are the simulated extinction spectra before (black) and after (red) conjugation: they are further discussed in the next section.

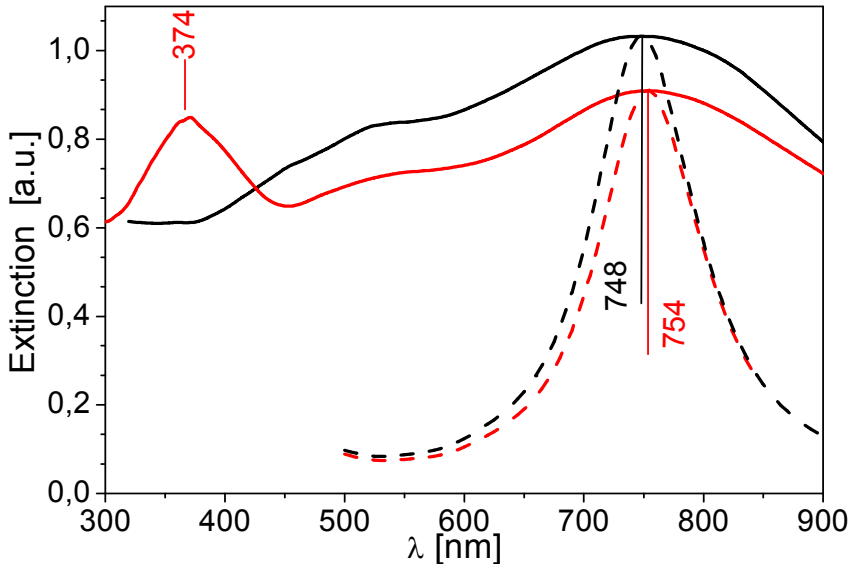

Figure 2: Experimental extinction spectra before and after conjugation are represented by the solid black and solid red lines, respectively. Theoretical extinction spectra before and after conjugation are represented by the dashed black and dashed red lines, respectively.

Two typical TEM micrographs of NAFTA6-conjugated NCs are reported in Figure 3A, showing nanostructures with truncated corners, hollow interiors and quite uniform and homogeneous porous walls. The statistical analysis provided average diameter and wall thickness of 50 nm and 5 nm, respectively.

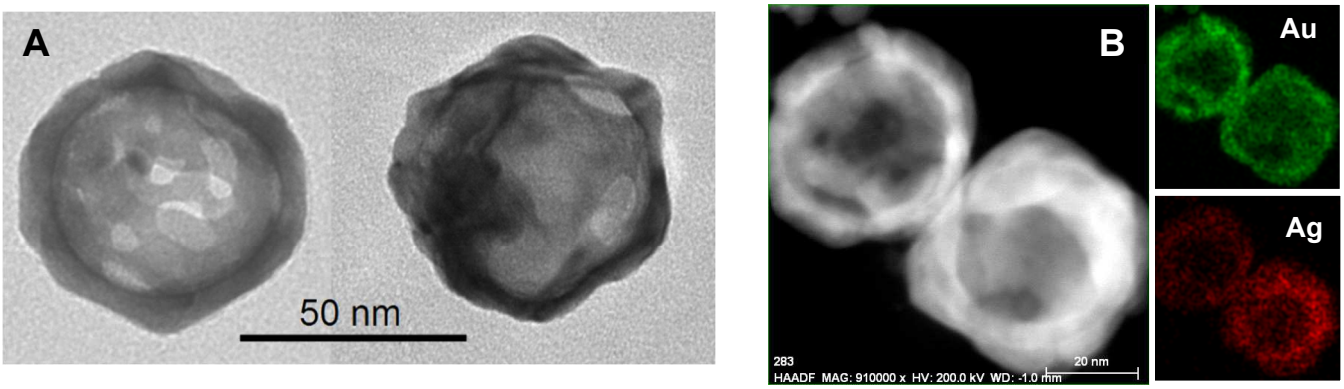

Figure 3: A) Typical TEM micrographs of two NCs. B) HAADF image of a pair of NCs (left) and STEM-EDS mapping of Au (upper right) and Ag (lower right).

Figure 3B shows typical HAADF-STEM images of the NCs. The hollow interior and the cage-like structure with porous walls are clearly visible. STEM-EDS analysis reported in Figure 3B, namely the elemental maps of Au (Au-L) and Ag (Ag-K), reveals the distribution of Ag and Au throughout the structures and shows formation of a Au/Ag alloy. However, as expected from the synthesis procedure,[7,10] there is an Au-rich region in the shell.[32] This also appears in the HAADF image from the increased contrast of the outer NC region, in comparison to the rest of the structure. Indeed, since the contrast is related with the difference in atomic weight between Ag and Au (Intensity proportional to $Z^{1.42}$, $Z_{Au} - 79$ vs $Z_{Ag} - 47$),[33] its increase observed at the surface can be attributed to a higher Au percentage in the nanoalloy.

The average composition of the NCs was evaluated by ICP-AES analysis, which gave 52% Au and 48% Ag. This datum was confirmed by microanalysis performed on test NCs with the STEM-EDS analysis.

Theoretical modelling

Single nanocages

On the basis of TEM/STEM images, we modeled a typical NC with a hollow truncated octahedron having 50 nm size and 5 nm shell thickness. Its faces are pierced in the center and its edges are rounded with 2 nm curvature radius (1 nm at the hole edges). Another important parameter in defining the optical properties of NCs is the size of the pores: since it cannot be accurately measured by TEM, it was used in the following as an adjustable parameter to match the experimental extinction peak wavelength. The model NC used in the simulation is represented in Figure 4.

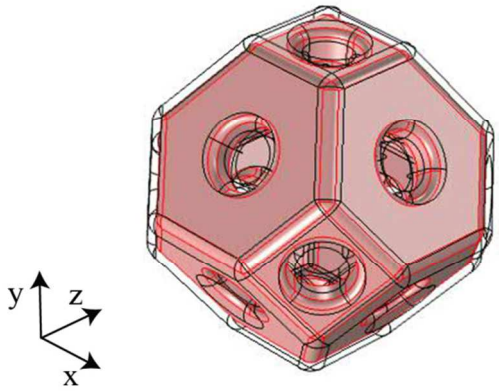

Figure 4: Example of model structure used in the simulations consisting of a pierced NC (pink) and a NAFTA6 shell (black lines).

The NAFTA6 shell surrounding the NC is represented in Figure 4 by the black line-delimited outer layer and it is positioned at 1.7 nm distance from the metallic surface. This distance roughly corresponds to the expected length of the molecule, evaluated by considering the typical interatomic distances.[34] The x axis indicates the light propagation direction and the E field is along the z axis. We fixed the refractive index of the environment to that of water, i.e. 1.33.

The dielectric constant of the metal was modeled according to the results of ICP-AES and STEM analysis, namely neglecting the small radial Au concentration gradient shown in Fig. 3B and assuming that gold and silver are homogeneously mixed in a solid solution:

$$\varepsilon_{NC} = 0.52\varepsilon_{Au} + 0.48\varepsilon_{Ag} \quad \text{Eq 1}$$

where ε_{Au} and ε_{Ag} are the bulk dielectric constants from Johnson and Christy.[35]

Since our Raman tests were performed at 650-800 nm, this approximation is expected to be good,[36] provided that a term due to the local wall scattering is added to the imaginary part of bulk ε:

$$\varepsilon_{Re} \approx \varepsilon_{Re}^{bulk}$$

$$\varepsilon_{Im} \approx \varepsilon_{Im}^{bulk} + \frac{Av_F\omega_p^2}{L_{eff}\omega^3} \quad \text{Eq 2}$$

where A =1, v_F is the Fermi velocity, ω_p the plasma frequency, L_{eff} the effective mean free path of electrons in the nanoparticle, which we take equal to the thickness of NC shell.

First, we simulated the NC without functionalization and compared the result to the experimental spectrum of Figure 2. The porosity level (that is the fraction of the NC surface area occupied by holes) was tuned in order to fit the observed plasmon peak position at 748 nm. By setting it at 19.5% we found the theoretical extinction reported in Figure 2 (dashed black line). Then, we added a layer of NAFTA6 to the model NC and repeated the calculations. Since the dielectric constant and filling factor of the dielectric layer are unknown, we varied the effective index of the functionalizing layer (n_{eff}) until the plasmon resonance of the functionalized NC was positioned on the experimental value of 754 nm (dashed red line in Figure 2). This gave a n_{eff} value of 1.38.

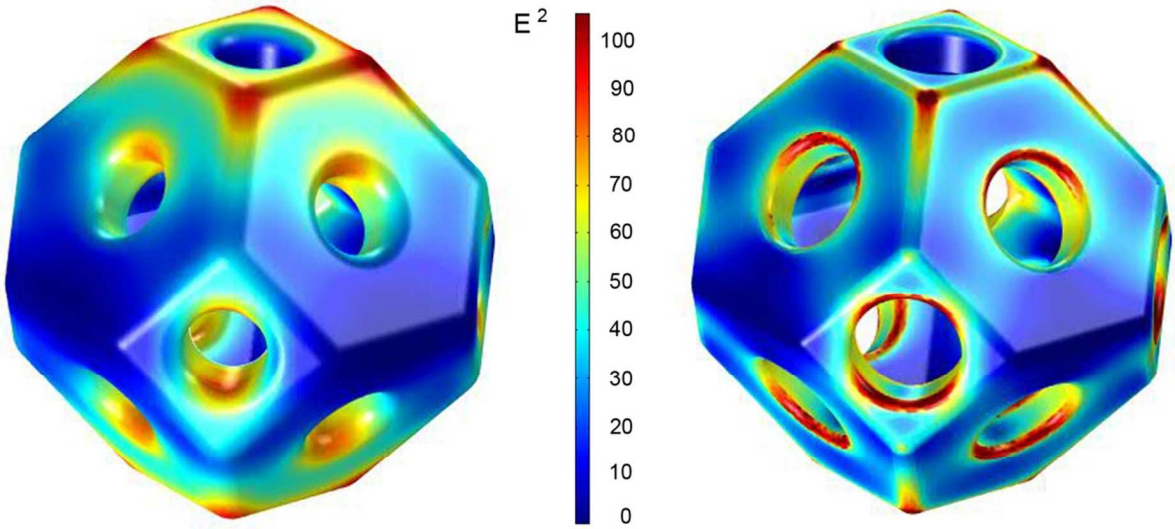

Figure 5: Field intensity distribution at plasmon resonance (λ=754nm) on the NC surface (right) and at 1.3 nm from the metallic surface (left).

Subsequently, we evaluated the electromagnetic field distribution around our model NC. Figure 5 shows the field intensity distribution at plasmon resonance on the NAFTA6-functionalized NC surface (right) and at 1.3 nm distance from it (left). This latter condition will be considered in the following calculations. In fact, the 1.3 nm distance corresponds to the position of the naphthalene ring of NAFTA6, whose vibrational modes are excited during the Raman experiments.[31] It was evaluated by supposing that NAFTA6 adsorption to the metallic surface maintains the CH_2 chain straight, as depicted in Figure 1.

It was then possible to calculate the theoretical SERS EF of the model NC:[37]

$$EF(\lambda_{inc}) = \frac{|\bar{E}_{shell}(\lambda_{inc})|^2}{|E_{inc}|^2} \frac{|\bar{E}_{shell}(\lambda_{Raman})|^2}{|E_{inc}|^2} \quad \text{Eq. 4}$$

where $|E_{inc}|^2$ is the intensity of the incident radiation, $|\bar{E}_{shell}(\lambda_{inc})|^2$ and $|\bar{E}_{shell}(\lambda_{Raman})|^2$ are the local field intensities averaged on the NC surface at the incident and Raman wavelength, respectively. The results are sketched in Figure 6, that shows the calculated extinction spectrum normalized to 1 (solid black line), the surface averaged field intensity at the incident wavelength (dashed green) and at the Raman Stokes wavelength corresponding to 1595 cm^{-1} shift (dashed red), and the EF (dashed black).

Simulations indicate that the local field intensity at the excitation wavelength follows the extinction spectrum: to the best of our knowledge this is the first result of modeling the spectral distribution of the local field intensity of large porous nanostructures. The fact that EF turns out to be blue-shifted with respect to the extinction spectrum depends on the fact that it is proportional to the product $E^2(\lambda_{inc}) \cdot E^2(\lambda_{Raman})$ and not merely to $E^4(\lambda_{inc})$: being $\lambda_{Raman} > \lambda_{inc}$ the product peaks at lower wavelength if plotted against λ_{inc}. This effect is well-known and has been demonstrated experimentally in Ref. 20.

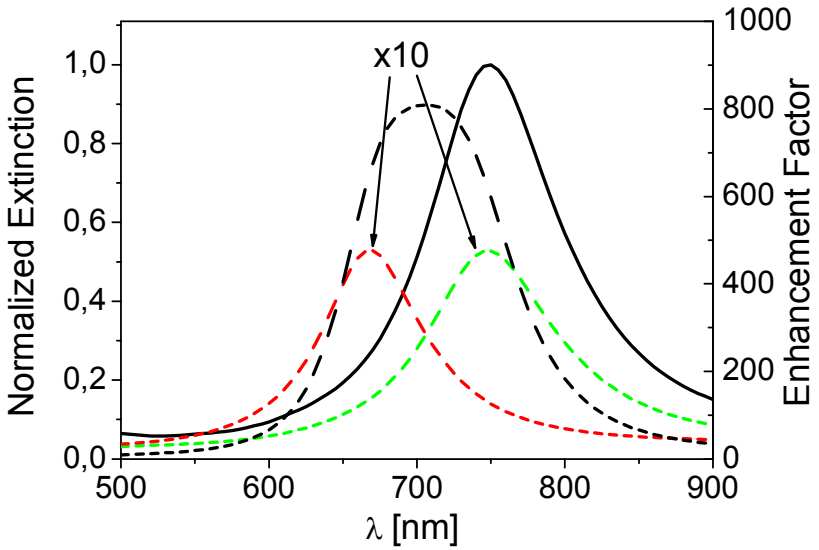

Figure 6: Calculated extinction spectrum (solid black line); calculated averaged field intensities at incident wavelength (dashed green) and at the Raman Stokes wavelength corresponding to the 1595 cm^{-1} shift (dashed red); calculated SERS EF profile (dashed black line).

The experimental spectrum in Figure 2 exhibits a large broadening with respect to the calculated one: this is due to the overlap of the contribution of NCs with different morphology and, possibly, also different alloy composition. Since TEM analysis revealed some degree of dispersion in the NCs size and shell thickness, it is likely that all geometrical parameters play a role in the broadening: in fact the literature shows that the peak position of the extinction is very sensitive both to pore size and to (NC size)/(shell thickness) ratio.[12,38,39] For example in Ref. 12 Mahmoud showed by means of DDA calculations that nanoframes (empty cubes with no faces, only the frame is present) with the same size exhibit a red-shift in the extinction spectrum when the frame thickness decreases; analogously in Ref. 38 Au showed that for nanoframes, the plasmon resonance peak red-shifts with increasing the ratio between the

cube side and the frame thickness. The effect of the pore sizes has been studied by Liaw, who showed that the larger the porosity, the higher the red-shift of the extinction peak.[39] The alloy composition can contribute as well to the spectral broadening in two ways: as a consequence of an inhomogeneous distribution of the metals in the alloy (HAADF-STEM gave evidence of a slightly higher concentration of Au in outer part of the NC) and as a distribution in the relative percentage of the two metals (ICP-AES can only measure the average value). We are assuming that a change in composition, and therefore in the dielectric constant of the alloy, causes a shift in the plasmonic resonance of the NCs as it is well known in the case of filled NPs. In the synthesis procedure of NCs, the elemental composition of the NCs and their porosity are always closely related and non-separable, since the galvanic replacement reaction occurring between the Ag NPs and the $HAuCl_4$ implies a simultaneous change in the alloy composition (that becomes richer in Au) and an increase in the porosity, leading to an overall red-shift of the extinction.[40] Due to the complexity of the problem, we attempted to tackle the effects of polydispersion on a merely qualitative fashion, by considering the experimental sample as an ensemble of nanoparticles, differing only in the pore size, that is a very critical parameter to control in the synthesis and cannot be easily evaluated by TEM. In this hypothesis, the experimental extinction spectrum and the corresponding SERS EF profile can be written as:

$$Ext(\lambda) = \sum_i \alpha_i Ext(i,\lambda) \qquad EF(\lambda) = \sum_i \alpha_i EF(i,\lambda)$$

where $Ext(i,\lambda)$ is the extinction spectrum of the NC with porosity level "i", $EF(i,\lambda)$ the associated SERS EF profile and α_i is the weight in the linear combination. A set of NCs with different degrees of porosity (0%, 5%, 9%, 13%, 16%, 19.5%, 24.5%, 30 %, 40%) was adopted and the $Ext(i,\lambda)$ and $EF(i,\lambda)$ were calculated for all of them. The weights α_i were determined from the fit of the experimental extinction spectrum and then used to work out its corresponding SERS EF profile.

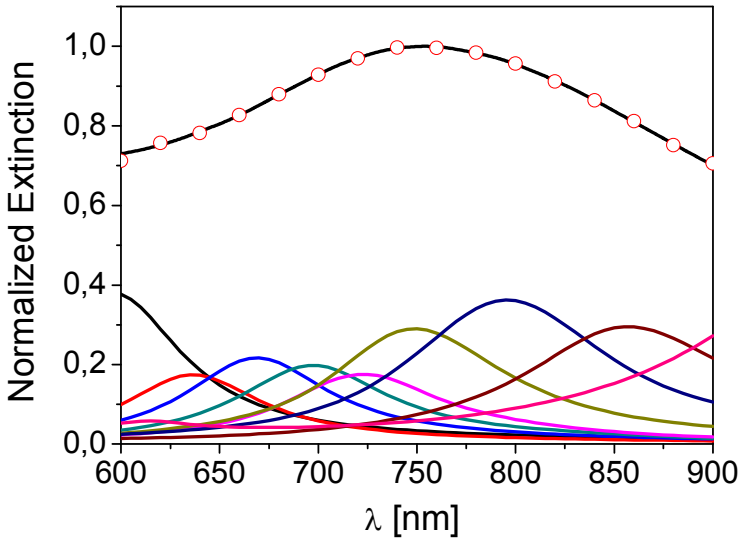

Figure 7: Normalized experimental extinction spectrum (solid black line); calculated extinction spectra of individual NCs with different pore sizes (continuous lines at the bottom: the higher the pore size, the longer the peak wavelength); fitting of the experimental extinction (red empty circles).

Figure 7 shows the experimental extinction spectrum (solid black line) along with the simulated extinction spectra of individual NCs (solid lines at the bottom of the Figure). The extinction spectra exhibit an increasing red shift as the porosity increases. The fit is represented by the red empty circles superimposed to the black line. In Figure 8 the solid and dashed black lines represent the experimental extinction spectrum and its simulated SERS EF profile; the solid and dashed red lines represent the calculated extinction spectrum of the 19.5% porosity NC and its SERS EF profile. The latter data have been already reported in Figure 6 and are here displayed again for comparison with the polydispersed system.

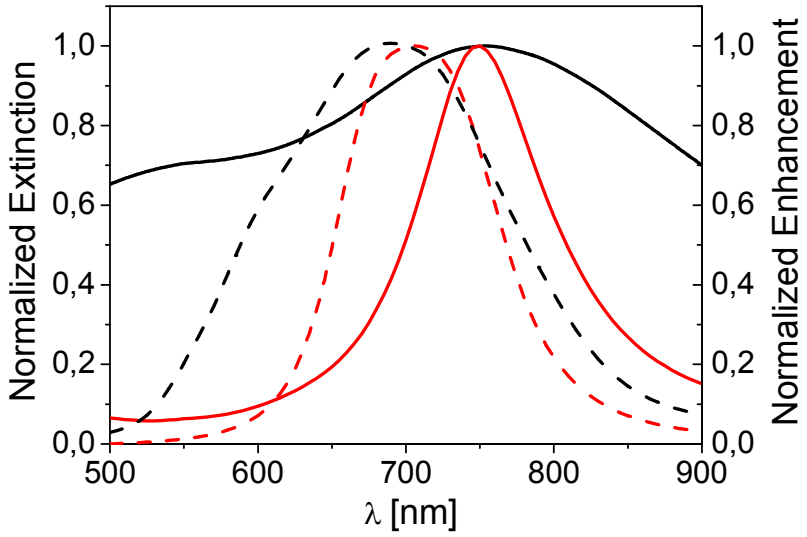

Figure 8: Experimental extinction spectrum (continous black line) and its corresponding calculated SERS EF profile (dashed black line). Calculated extinction spectrum of a single NC with 19.5 % porosity level (continous red line) and its corresponding calculated SERS EF (dashed red line).

As it can be noticed from Figure 8, the SERS EF profile of the polydisperse system turns out to have similar features compared to the case of the single NC with 19.5% porosity level. In fact, besides exhibiting some broadening, it still peaks at lower wavelength with respect to the extinction.

As a whole, the theoretical calculations indicate, as a qualitative guideline, that also in the presence of polydispersion the SERS EF profile should be somewhat blue-shifted with respect to the extinction spectrum. The exact amount of such shift is evidently not quantifiable with the present approach.

Dimers of nanocages

In this section we present the calculation of the extinction and the local field enhancement in dimers of identical NCs, with different gap sizes. The NCs that form the dimer have been chosen with the same alloy composition and the same model structure as the ones studied in the previous section; the porosity level has been set at 19.5%. The NCs are arranged as illustrated in Figure 9 and the electric field is polarized along the dimer axis. The extinction spectra and the surface averaged near-field enhancement at 1.3 nm from the surface, $\langle\left(\frac{E}{E_0}\right)^4\rangle$, are reported in Figure 10 A and C, respectively. The black line refers to an isolated NC; the

red, green and blue ones to dimers with a 20, 10 and 4 nm gap, respectively. Extinction data for the dimer are divided by 2 (number of particle in the dimer) and then normalized to the maximum of the isolated NC.

For the sake of comparison, the same calculations were repeated for dimers formed by filled spheres. These spheres have been modelled with the same alloy composition and the same total surface area as the NCs; the electric field is again polarized along the main axis. Results are shown in Figure 10 B and D: the color code and the normalization procedure are analogous to the ones adopted in Figure 10 A and C.

The most significant results from the simulations can be summarized in the following points:

- NC dimers exhibit a red-shift of both extinction and near field-spectrum (with respect to the isolate NC) that increases reducing the gap size. This behavior qualitatively reproduces what happens with dimers formed by filled nanospheres.
- An important difference, however, comes to light when one looks at the ratio between the surface averaged near-field enhancement ($\langle\langle\left(\frac{E}{E_0}\right)^4\rangle\rangle$) maximum of the 4 nm gap dimer and of the isolated NP: in fact this amounts to 2 for a NC dimer and to 45 for a filled nanosphere dimer. This finding evidences that a NC dimer is only marginally more efficient in amplifying the field with respect to the isolated NC; instead a remarkably larger effect is observed in the case of filled nanospheres.

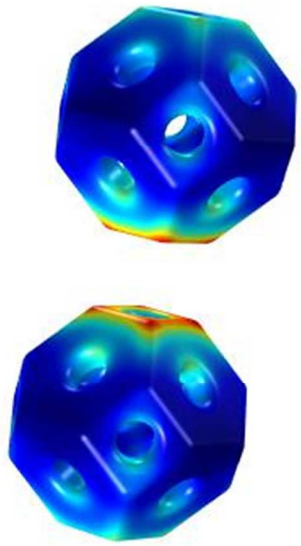

Figure 9: Spatial arrangement of the NCs in the dimer.

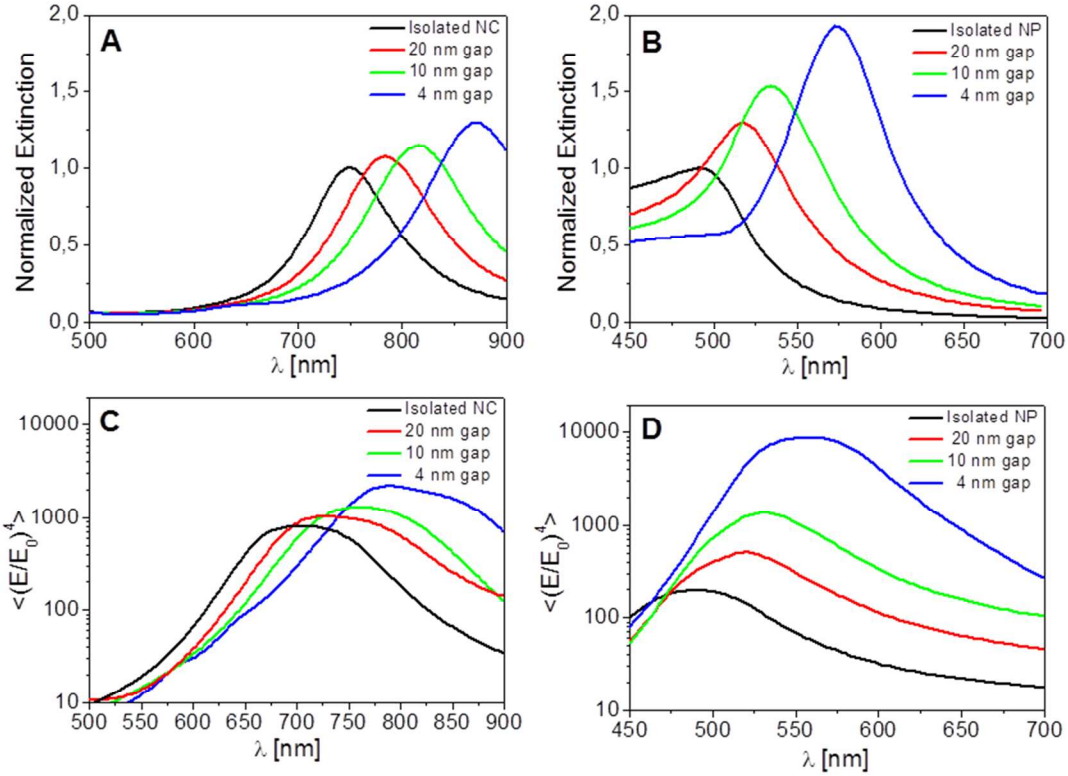

Figure 10: Calculated data for the dimer of NCs are reported in the left column, where A shows the extinction spectra and C the surface averaged near-field enhancement. The black line represent the isolated NC, the red, green and blue ones are the dimer with 20, 10 and 4 nm gap respectively. Extinction spectra are divided by two

and then normalized to the maximum extinction of the isolated NC. Identical normalization procedure and color code are used for the dimer of filled spherical NPs, reported in B and D.

Raman measurements

WS-SERS measurements were carried out on NAFTA6@NCs in order to determine the wavelength dispersion of the field enhancement (EF). It is worth noting that NAFTA6 has an absorption band at about 370 nm and therefore Raman resonance contributions are avoided throughout the explored excitation wavelength range.

Figure 11 reports the Raman spectrum of NAFTA6 powders at 785 nm excitation. According to Ref. 41, the most intense bands correspond to the vibrational modes of naphthalene. In particular, the two low frequency bands at 510 and 615 cm^{-1} are assigned to ring bending modes and the one at 1403 cm^{-1} and the doublet at 1586,1595 cm^{-1} to ring stretching modes. The band at 1693 cm^{-1} is due to the C=O stretching mode.

Figure 12A shows the Raman spectra of NAFTA6 in acetone (black) and of pure acetone (red). Figure 12B reports the Raman spectrum of NAFTA6 bound to NC in H_2O:acetone mixture (5:1). The excitation wavelength was 780 nm in both cases.

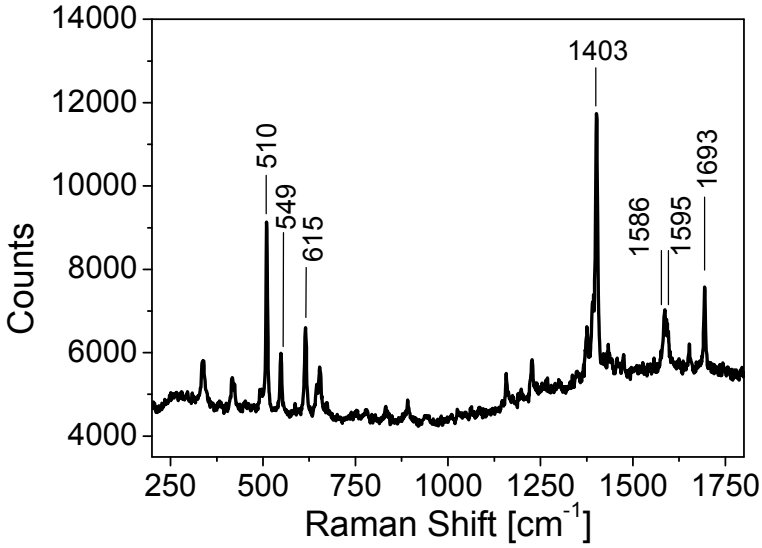

Figure 11: Raman spectrum of NAFTA6 powders at 785 nm excitation.

According to Ref 42 and 43, the acetone bands at 1361 and 1426 cm^{-1} are assigned to in-phase and out of phase CH_3 bending. When NAFTA6 is dissolved in acetone, its bands at 1375 cm^{-1} and 1400 cm^{-1} are visible only as shoulders of the solvent bands; on the other hand, the band at 1595 cm^{-1} (which appears as a single broadened band instead of the doublet observed in the powder spectrum) is clearly identifiable and therefore it was used as a reference to work out the experimental EF.

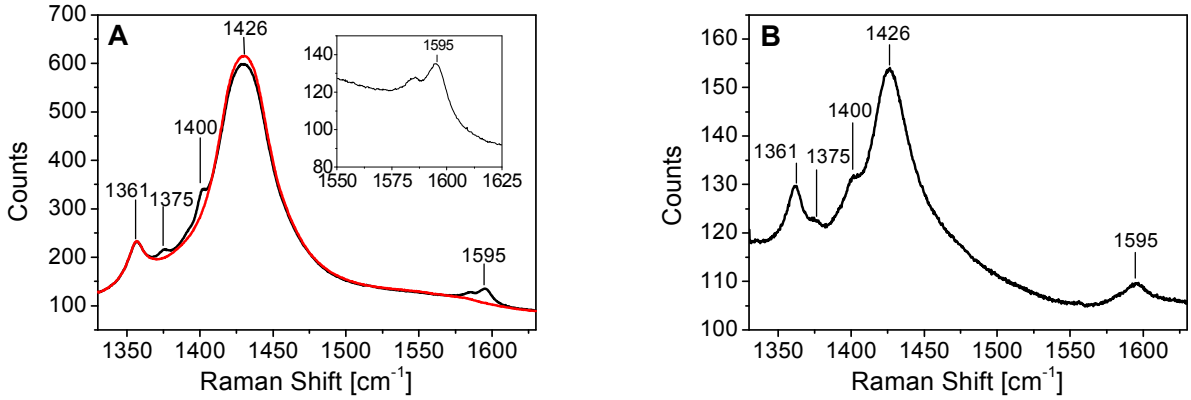

Figure 12: A) Raman spectrum of NAFTA6 in acetone (black) and pure acetone (red) at 780 nm excitation. Inset: enlargement around 1600 cm^{-1} B) SERS spectrum of NAFTA6@NC in 5:1 H_2O:acetone mixture at 780 nm excitation.

We made use of the following definition:[37]

$$EF(\lambda_{inc}) = \frac{I_{SERS}}{I_{Raman}} \frac{C_{NAFTA6}}{C_{\mathrm{NAFTA6@NC}}} \quad \text{Eq. 5}$$

where I_{SERS} is the integrated area of the 1595 cm^{-1} Raman peak of NAFTA6@NC and I_{Raman} is the area of the same peak in the reference solution. $C_{\mathrm{NAFTA6@NC}}$ and C_{NAFTA6} are the concentration of NAFTA6 in the sample and in the reference solution, respectively. We used 10^{-2} M NAFTA6 in acetone as reference solution. The procedure used to estimate the error bars in given in the Supplementary Information.

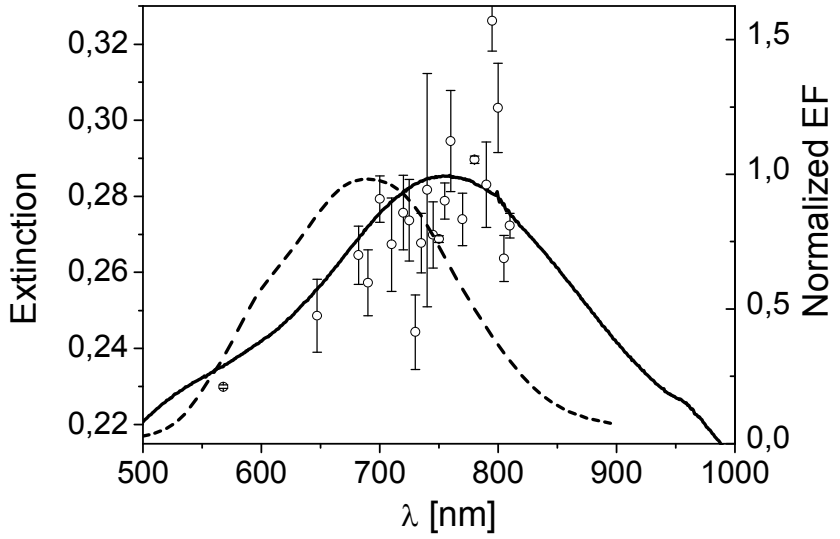

Figure 13: Extinction spectrum of NAFTA6@NC (solid black line); normalized experimental SERS EF profile (empty circles); normalized calculated SERS EF profile for the polydispersed system (dashed line).

Figure 13 shows the experimental extinction spectrum (solid black line), the normalized experimental SERS EF profile (empty circles)[44] and the normalized calculated SERS EF profile for the polydispersed system (dashed line): the experimental SERS EF profile has been numerically corrected to account for self-absorption[45] (see details in Supplementary Information). Notice that the trend is not smooth but neighboring data points fluctuate noticeably: this is due to the fact that the background subtraction was rather difficult, since the latter was not flat and the peak at 1595 cm^{-1} quite small. Repeatability of the measurements was checked as well: excitation wavelengths 568, 647, 720, 780, 800 nm were repeated twice and 700 nm was repeated 4 times throughout the period of measurements, showing in all

cases that data were consistent within 20%. On the basis of these data we can rule out any possible reshaping of the NCs with the level of laser irradiation used in our experiments.

A trend can be spotted in SERS EF profile by focusing on the data with the smallest error bars: the profile rises from 580 nm to about 700 nm and then it flattens out in the 700-800 nm region, where the extinction reaches a maximum.

Absolute values of the experimental EF amount to about 40 at maximum and therefore exhibit a rather large difference with respect to the simulations in Figure 6: we suggest that polydispersivity of NCs may be responsible for such discrepancy. In fact, considering the extinction spectrum as the sum of narrower spectra corresponding to subgroups of NCs with different geometrical/compositional parameters, it is expected that each subgroup will contribute differently to the collected SERS signal for a certain excitation wavelength. In this respect, NCs peaking at a certain wavelength will be excited much more efficiently than the others. However, since the experimentally recorded Raman signal is normalized to the total amount of dye and not to the quantity absorbed on the most efficiently excited NC subgroup, this can be interpreted as an overestimation of $C_{NAFTA6@NC}$, making the experimental enhancements predictably smaller than the theoretical ones. In addition, also the choice of geometrical parameters, that are not all accurately measurable experimentally, may alter the theoretical estimation of the absolute value of EF.

4. Discussion

As already mentioned in the introduction, the experimental SERS EF profile of colloidal solutions of NPs always lies strongly to the red with respect to the plasmon band of individual NPs. [24,25,26,27,28,46] This is commonly attributed to the presence of aggregates. The key point is the well-recognised hurdle that experimentalists face in preparing colloidal solutions containing only isolated NPs, associated to the extreme sensitivity of SERS to aggregates. In this regard, Moskovits pointed out that even when a TEM analysis does not evidence the presence of clusters, their contribution can still be dominant in the solution.[29] Aggregates influence the experimental results through a combination of three factors:

a) Tiny gaps (formed among clustered NPs) amplify the SERS signal up to several orders of magnitude more efficiently then isolated NPs.[18,29,37] Le Ru in Ref 37 showed that a dimer of silver NP with a 2 nm gap amplifies the (surface averaged) local field about 100 times more strongly than an isolated NP.
b) Extinction cross sections are much less sensitive than SERS signal to the aggregation.[18]
c) With respect to isolated NPs, tiny gaps become resonant at longer wavelengths.[37]

Therefore, in presence of a small amount of aggregates, the extinction spectrum is dominated by isolated NPs, while the contribution to SERS arises mostly from aggregates and in a red-shifted spectral region. As an example, we mention the study carried out in Ref 24. The authors synthesized several samples by adding a SERS probe to colloidal solutions of Silver NPs: in the least aggregated one the extinction spectrum showed only the plasmon peak of Ag NP at about 400 nm without any appreciable shoulder in the red part of the spectrum due to clustering. In spite of this low level of aggregation, which did not appear in the extinction spectrum, the authors found the SERS signal peaking about 200 nm more to the red with respect to the extinction. Furthermore, the extinction spectrum and the SERS EF profile did not match at all, since the extinction above 400 nm sharply decreased, while the SERS profile grew from 425 nm onwards until it reached a maximum at about 625 nm. Indeed, an extensive TEM analysis revealed that 97.2% of the NPs appeared non-aggregated, while 2.8% appeared aggregated on the TEM grid. Clearly, in solution the percentage of aggregates could be much lower than that measured on the TEM grid. From

554 these data the authors inferred that the Raman signal was mainly due to the tiny amount of
555 aggregated nanoparticles, rather than to the majority of non-aggregated ones.

556 An in-depth analysis of our data in Figure 13 reveals some differences with respect to
557 the previously mentioned literature. The SERS EF profile in the presence of aggregates is
558 expected to rise steeply above the extinction maximum, towards the spectral region were
559 aggregates absorb (notice that our calculations show that also dimers of NCs peak at longer
560 wavelength with respect to isolated NC and further proof of this can be found in the
561 experimental papers by Mahmoud[12,47]). On the contrary, our data tend to flatten out around
562 the region of the extinction maximum. Moreover, the observed absolute values are very low
563 throughout the explored spectral region, that is more than 250 nm wide.

564 In order to interpret these data, we can envision two limit explanations, that is a) some
565 aggregates of NCs are present in solution but they behave differently with respect to
566 aggregates of filled NPs and b) no aggregates are present in solution. Concerning the point
567 a), our calculations evidence that a dimer of NCs is remarkably less efficient in amplifying the
568 local field than a dimer of filled NPs (compared to the corresponding isolated NPs).Therefore
569 WS-SERS measurements are expected to be less influenced by the presence of aggregates
570 in a NCs solution with respect to a filled NP solution. Papers in the literature confirm that the
571 effect of aggregation among hollow NPs is much less predictable than in the case of their
572 filled counterparts. For example, the SERS response of hollow NPs has been extensively
573 studied by Mahmoud at different and controlled degrees of aggregation in Langmuir-Blodgett
574 assembled monolayers:[12] he showed that 80 nm gold nanoframes exhibit a unique behaviour
575 upon aggregation, inhibiting the SERS signal rather than strongly increasing it. This has been
576 attributed to a reduction of the inner field upon interaction, not compensated by the inter-
577 particle field increase. Concerning point b), it is difficult to experimentally ascertain that no
578 aggregates populate the laser focus during the SERS measurements. Their effect is normally
579 recognized a posteriori as deviations from the expected behavior of an isolated NP. In this
580 respect we may rely on the results of our simulations that predicted a SERS EF profile blue-
581 shifted with respect to the extinction: since we do not observe it, this would indicate that some
582 form of aggregation is present in solution. In addition, Figure 6 of the Supplementary
583 Information shows that dimers and trimers of NCs can be found on the TEM grid, even though
584 this cannot be regarded as a definitive proof of their presence in solution.

Summarizing, our experimental evidence is that the SERS signal, in this system, is distributed around the extinction spectrum, unlike what is always observed for colloidal solution of NPs. With the help of simulations, we have tried to draw a microscopic picture of the system to explain our findings. We propose that the observed SERS trend is the result of the isolated particle behaviour (that would blue-shift the SERS EF profile with respect to the extinction) and of the presence of aggregates (that would strongly red-shift the SERS EF profile with respect to the extinction). Considering that aggregates between NCs are only slightly more efficient in amplifying the local field than isolated NCs, the final result turns out to be a correlation between SERS EF profile and extinction. We point out that this is probably accidental, being due to a combination of two counteracting effects in a very complex system.

5. Conclusions

Chitosan protected NCs have been synthesized by a galvanic replacement-based procedure, functionalized with the Raman reporter molecule NAFTA6 and characterized by TEM, STEM and ICP. NAFTA6@NC have been extensively purified by multiple dialysis steps.

FEM simulation have been used to predict the near- and far- field properties of an isolated NC and showed that the near-field follows the same spectral dependence as the far field (extinction) spectrum. The SERS EF profile as a function of the excitation wavelength, therefore, peaks at a higher energy with respect to extinction. The single NC spectrum turns out to be remarkably narrower than the experimental one, indicating that our NC colloidal sample is substantially polydispersed. This originates from a size distribution in the geometrical parameters of the NCs and, possibly, in the alloy composition, as evidenced by a TEM and a STEM-EDS analysis, respectively. A qualitative attempt has been undertaken in order to bridge the gap between the single particle simulations and the experimental system: the experimental spectrum has been fitted by summing up weighted contributions from individual NCs with different porosity (and therefore different extinction maximum), and the same combination of NCs was used to work out the SERS EF profile. This model suggests that the SERS EF profile should be blue-shifted with respect to the extinction also in the presence of polydispersivity. FEM simulations have been used to model also the properties of NC dimers, in particular their extinction and near-field spectrum, as a function of the gap size. It turned out that, reducing the gap, both spectra shift to the red with respect to the isolated NC, in analogy to what happens with filled NP dimers. Moreover, while the field enhancement in a filled NP dimer is remarkably larger compared to the single NP, the enhancement in a NC dimer is instead only slightly larger with respect to the isolated NC.

In the experimental section, we probed the local field enhancement of a solution of NCs by using Wavelength Scanned SERS. The experimental data showed that the local field is distributed in the same spectral region as the extinction and that the absolute value of the enhancement factor remains very low throughout the spectral region explored (568-800 nm). This behavior differ from what observed in literature for filled NPs, where the local field enhancement lies strongly red-shifted with respect to the extinction due to the unavoidable presence of aggregates.

We propose, with the help of simulation results, that this different behavoiur arises from the limited increase in local field amplification that NCs exhibit upon aggregation, opposite to the case of filled NPs in which clustering strongly raise the local field compared to the isolate NP.

Lastly, the present study provides a combined theoretical and experimental investigation of a basic and widely debated issue, which has not been tackled by many papers, probably due to the experimental difficulty in measuring the local field dispersion. We think that our study, beside fundamental aspects, can also have practical implications in fields where the peculiar features of NCs - namely, the empty inner space that can carry active moieties and their plasmonic maximum in the spectral window of transparency of biological tissue - can be exploited, for example in drug delivery applications, where surface enhanced spectroscopies can be applied to localize and monitor the ongoing release process.

Acknowledgments

The authors gratefully acknowledge financial support from PRIN 2009 prot. 2009YSP28A_001 and from Fondazione Cariparo (Progetti Eccellenza 2008) through the grant “Surface PLasmonics for Enhanced Nano Detectors and Innovative Devices” (SPLENDID).

The authors also express their thanks to:

Dr. R. Traversi of the Chemistry Department of the University of Firenze, Italy for ICP analysis; the Institute of Organic Chemistry with Centre of Phytochemistry BAS, Sofia, Bulgaria and, in particular, to Prof. I. Timtcheva and Dr. G. Dobrikov, for providing the reporter molecule; Dr. G. Mattei, Department of Physics, University of Padova, Italy and Prof. G. Dellepiane, University of Genova, Italy for useful discussions.

651 ## Notes and references

1 M.B. Cortie and A.M. McDonagh, *Chem. Rev.*, 2011, **111** (6), 3713.

2 S. Eustis and M.A. El-Sayed, *Chem. Soc. Rev*., 2006, **35**, 209.

3 S. Tokonami, Y. Yamamoto, H. Shiigi and T. Nagaoka, *Analytica Chimica Acta*, 2012, **716**, 76.

4 M.C. Daniel and D. Astruc, *Chem. Rev.*, 2004, **104**, 293.

5 M.S. Yavuz, Y. Cheng, J. Chen, C.M. Cobley, Q. Zhang, M. Rycenga, J. Xie, C. Kim, K.H. Song, A.G. Schwartz, L.V. Wang and Y. Xia, *Nature Materials*, 2009, **8**, 935.

6 L. Tian, N. Gandra and S. Singamaneni, *ACS Nano*, 2013, **7** (5) 4252.

7 J. Chen, B. Wiley, Z.Y. Li, D. Campbell, F. Saeki, H. Cang, L. Au, J. Lee, X. Li and Y. Xia, *Adv. Mater.*, 2005, **17**, 2255.

8 S.E. Skrabalak, J. Chen, L. Au, X. Lu, X. Li and Y. Xia, *Adv. Mat*., 2007, **19**, 3177.

9 Y.S. Zhang, Y. Wang, L. Wang, Y. Wang, X. Cai, C. Zhang, L.V. Wang and Y. Xia, *Theranostics*, 2013, **3** (8), 532.

10 B.N. Khlebtsova, V.A. Khanadeevb, I.L. Maksimovab, G.S. Terentyukc and N.G. Khlebtsova, *Nanotechnologies in Russia*, 2010, Vol. 5 Nos. 7–8, pp 454–468.

11 J. Chen, D. Wang, J. Xi, L. Au, A. Siekkinen, A. Warsen, Z.Y. Li, H. Zhang, Y. Xia and X. Li, *Nano Lett.*, 2007, **7** (5), 1318.

12 M.A. Mahmoud, B. Snyder and M.A. El-Sayed, *J. Phys. Chem. C*, 2010, **114**, 7436.

13 A.M. Schwartzberg, *Anal. Chem.*, 2006, **78**, 4732.

14 M.A. Mahmoud, *Langmuir*, 2013, **29**, 6253.

15 M. Alloisio, A. Demartini, C. Cuniberti, G. Dellepiane, S. Jadhav, S. Thea, E. Giorgetti, C. Gellini, M. Muniz-Miranda, *J. Phys. Chem. C*, 2009, **113**, 19475.

16 M. Alloisio, A. Demartini, C. Cuniberti, G. Petrillo, E. Giorgetti, A. Giusti and G. Dellepiane, *J. Phys. Chem. C*, 2007, **111**, 345.

17 G.D. Moon, S.W. Choi, X. Cai, W. Li, E.C. Cho, U. Jeong, L.V. Wang, and Y. Xia, *J. Am. Chem. Soc.*, 2011, **133**, 4762.

18 E.C. Le Ru, C. Galloway and P. G. Etchegoin, *Phys. Chem. Chem. Phys.*, 2006, **8**, 3083.

19 S.L. Kleinman, B. Sharma, M.G. Blaber, A.I. Henry, N. Valley, R.G. Freeman, M.J. Natan, G.C. Schatz and R.P. Van Duyne, *J. Am. Chem. Soc.,* 2013, **135**, 301.

20 A.D. McFarland, M.A. Young, J.A. Dieringer and R.P. Van Duyne, *J. Phys. Chem. B*, 2005, **109**, 11279.

21 V. Weber, A. Feis, C. Gellini, R. Pilot, P. R. Salvi and R. Signorini, *Phys. Chem. Chem. Phys.,* 2015, DOI: 10.1039/C4CP05054A.

22 B.J. Messinger, K.U. von Raben, R.K. Chang and P.W. Barber, *Phys. Rev. B*, 1981, **24** (2) 649.

23 N. Félidj, J. Aubard, G. Levi, J. R. Krenn, A. Hohenau, G. Schider, A. Leitner and F. R. Aussenegg, *Appl. Phys. Lett.*, 2003, **82**, 3095.

24 K.U. Von Raben, R.K. Chang, B.L. Laube and P.W. Barber, *J. Phys. Chem.*, 1984, **88**, 5290.

25 D. Fornasiero and F. Grieser, *J. Chem. Phys.*, 1987, **87**, 3213.

26 H. Feilchenfeld and O. Siiman, *J. Phys. Chem.*, 1986, **90**, 2163.

27 M. Kerker, 0. Siiman and D.S. Wang, *J Phys. Chem.*, 1984, **88**, 3168.

28 E.C. Le Ru, M. Dalley and P.G. Etchegoin, *Current Applied Physics*, 2006, **6**, 411.

29 M. Moskovits, *J. Raman Spectrosc.*, 2005, **36**, 485.

30 S. Trigari, A. Rindi, G. Margheri, S. Sottini, G. Dellepiane and E. Giorgetti, *J. Mater. Chem.*, 2011, **21**, 6531.

31 A. Zoppi, S. Trigari, E. Giorgetti, M. Muniz Miranda, M. Alloisio, A. Demartini, G. Dellepiane, S. Thea, G. Dobrikov and I. Timtcheva, *J. of Colloids and Interface Science*, 2013, **407**, 89.

32 W. Li, L. Kuai, L. Chen and B. Geng, *Sci Rep.*, 2013, **3**, 2377.

33 F.L. Deepak, J. Rivas and M.J. Yacamán, *IOP Conf. Ser.: Mater. Sci. and Eng.*, 2014, **55**, 012005.

34 F.H. Allen, D.G. Watson, L. Brammer, A.G. Orpen and R. Taylor, “Typical interatomic distances: organic compounds“, in International Tables for Crystallography, 2006, vol. C, chapter 9.5, pp790-811.

35 P.B. Johnson and R.W. Christy, *Phys. Rev. B*, 1972, **6**, 4370.

36 M. Moskovits, I. Srnova-Sloufova and B. Vlckova, *J. Chem. Phys.*, 2002, **116**, 10435.

37 E.C. Le Ru and P.G. Etchegoin, *Principles of surface-enhanced Raman spectroscopy and related plasmonic effects*, 2009, Elsevier, Amsterdam.

38 L. Au, Y. Chen, F. Zhou, P.H.C. Camargo, B. Lim, Z.Y. Li, D.S. Ginger, Y. Xia, *Nano research*, 2008, **1**, 441.

39 J. W. Liaw, J. C. Cheng, C. Ma, and R. Zhang, J. Phys. Chem. C, 2013, 117, 19586.

40 Y. Sun and Y. Xia, Nano Lett., 2003, 3 (11), 1569.

41 E. Giorgetti, S. Trigari, A. Rindi, G. Margheri, S. Sottini, G. Dellepiane, G. Brusatin, L. Brigo, M. Muniz-Miranda and I. Timtcheva, *Phys. Status Solidi (b)*, 2012, **249**, 1188.

42 P.J. Larkin, "Infrared and Raman spectroscopy, principles and spectral interpretation", 2011, Elsevier, Amsterdam.

43 G. Dellepiane and J. Overend, *Spectrochimica acta*, 1966, **22**, 593.

44 The data have been normalized in the region where the trend reaches a plateau, as discussed later.

45 T. Van Dijk, S.T. Sivapalan, B.M. Devetter, T.K. Yang, M.V. Schulmerich, C.J. Murphy, R. Bhargava and P.S. Carney, *J. Phys. Chem. Lett.*, 2013, **4**, 1193.

46 M. Moskovits, *Phys. Chem. Chem. Phys.,* 2013, **15**, 5301.

47 M.A. Mahmoud, *NanoLett.*, 2009, **9**, 3025.